Desiccation shrinkage process in clayey soils experimental analysis from digital image correlation (DIC) technique results

Zhengtian YANG [1], Mahdia HATTAB [1], Mohamad JRAD [1]

[1] *Laboratoire d'Etude des Microstructures et de Mécanique des Matériaux, Université de Lorraine, CNRS UMR 7239, Arts et Métiers ParisTech, F-57000 Metz, France.*

RESUME

During the drying process, an initially saturated clay deforms mainly due to the loss of water. It causes clay shrinkage that represents one of the fundamental reasons of cracking by desiccation. It is of great interest to understand the desiccation process in such complex soils. The main point is that many properties of the material, such as water content distribution, displacement, strain and stress fields. The proposed method of analysis allows to understand more deeply the process of drying in clays including shrinkage, crack initiation and finally, crack network development. This research allows to go further in investigating the drying phenomenon in remolded and initially saturated kaolinitic clay.

Mots-clefs Kaolin, Desiccation shrinkage, Water content, Digital image correlation

I. INTRODUCTION

The mechanical behavior of clayey soils is significantly affected by water content, with desiccation, or the drainage of water through evaporation, being a common occurrence in geotechnical engineering. Desiccation often leads to shrinkage and cracking in clayey soils, posing challenges for the stability and performance of geotechnical structures such as slopes, embankments, and foundations (Morris et al. 1992, Nahlawi et al. 2004, Dyer 2005, Tang et al. 2011, Wang et al. 2016).

Several studies have explored the desiccation shrinkage of clayey soils (Haines, 1923, Stirk, 1954, Fleureau et al., 1993, Péron et al., 2007-2009, Tang et al., 2011, Tempany, 1917). Recent studies by Lu et al. (2005) and Tang et al. (2010, 2011) have explored the relationship between shrinkage, tensile strength, and microstructural variations. Drying in soils induces capillary tension and water menisci formation between particles (Taibi, 1994). Capillary tensions increase with water evaporation, leading to a decrease in pore radii following Jurin's Law (1718). In the context of continuous media mechanics, the increase in capillary stress during drying enhances the clay's strength, particularly its tensile strength (Lu et al., 2010).

Experimental determination of the shrinkage curve, expressed as void ratio versus water content, is achievable through various techniques imposing specific suctions on small material pieces (Fleureau et al., 1993). However, assessing shrinkage in the field or on large samples is challenging

due to medium heterogeneity and the heterogeneous evolution of water content and strains during drying. Different measurement techniques, including Laser, Computed Tomography, and Digital Image Correlation, have been utilized to capture specimen property variations during drying. For example, Péron et al. (2009c) analyzed global deformation in different directions on initially saturated rectangular clayey samples using a Teflon support to minimize frictional effects. Eid et al. (2015) and Wei et al. (2016) employed Digital Image Correlation to capture strains and displacements during desiccation.

The primary aim of this study was to understand and characterize desiccation shrinkage phenomena in clays through a comprehensive analysis of experimental results. Real-time measurements of physical variables such as water content, strain, and displacement fields provided detailed insights into the deformation process during drying. For this purpose, an initially saturated clay sample was analyzed during drying. The sample, a thin parallelepiped, was carefully prepared and placed on a smooth bottom plate with minimal friction at the clay/support interface to ensure conditions conducive to free desiccation shrinkage. Throughout drying, the deformation field of the clay was meticulously measured using Digital Image Correlation (DIC), a technique enabling precise identification of shrinkage evolution. These results facilitated an estimation of heterogeneous distribution the water content from the saturated to unsaturated.

II. MATERIAL AND EXPERIMENTAL METHODS

A. Material properties and specimen preparation

The soil selected for the study is an industrial clay called Kaolin K13 (from Sibelco, France). The geotechnical tests indicated that liquid and plastic limits were about 40% and 21%, respectively. The density of solid particles G_s is about 2.63. For the desiccation tests, the material was prepared following different steps. Initially the clay was in form of dry powder, it was then mixed with de-aired water to reach a water content of 1.2 times the liquid limit ($w = 1.2w_L$). The obtained slurry was mechanically stirred for at least 15 minutes with a velocity of 280 rpm, which ensures to evacuate remaining air bubbles. Then, the material was placed in a carefully sealed container for 24 hours, which allows to well homogenize its water content.

To perform Digital Image Correlation (DIC), a thin square surface clay sample was used. For this purpose, a square mold of 179 mm x 179 mm, and 5 mm in thickness was designed. The bottom of the mold, which is in fact the support of the sample, is a smooth plate of Teflon treated with a thin layer of grease, as recommended by Péron (2008). This set up allows to drastically minimize the friction developed during shrinkage at the interface between the clay mud and the support. The material was introduced in the mold, and afterwards the surface was treated with an appropriate speckle allowing to get different gray-scale levels between the speckle (with black color) and the original clay matrix (with much lighter color) as shown in Fig. 1.

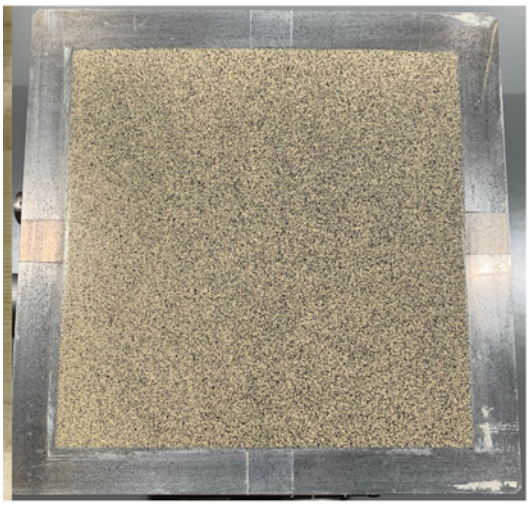

FIGURE 1. **Illustration of a speckle field on the specimen surface**

B. Test procedure for the shrinkage measurements

- Shrinkage curve

The Aiming to identify the water retention characteristics of the clay, and the shrinkage properties, tests on small samples were conducted involving measuring sample volumes (previously submitted to a given suction level) via hydrostatic weighing in liquid Kerdane. Samples were preconditioned to specific relative humidity (RH) levels using salt solutions in a desiccator. Five salts ($CaSO_4$, Na_2SO_4, NaCl, K_2CO_3, KOH) were employed to achieve the desired RH values (see Table 1). RH in the desiccator was monitored by a thermo-hygrometer, which also recorded temperature. These measurements made it possible to calculate the suction using Kelvin law Eq.1.

$$s = \frac{\rho_w RT}{M_w} \ln(RH) \qquad Eq.1$$

Where s is the suction in Pa; ρ_w is the density of water in kg/m^3; M_w is the molar mass of water in kg/mol; R is the ideal gas constant in $J/mol \cdot K$; T is the Kelvin temperature in K and RH is the relative humidity.

TABLE 1. **The salt solutions and the corresponding relative humidity and suction values**

Salt solutions	Relative humidity RH (%)	Suction (MPa)
$CaSO_4$	99.8	0.27
Na_2SO_4	92.5	10.5
NaCl	75.5	38
K_2CO_3	46.5	103.8
KOH	6.8	363.7

This method allows to obtain the Water Characteristic Curve (SWCC), by establishing relationships between the water content (w), the degree of saturation (S_r) and the suction (s), as well as the

shrinkage curve relating the void ratio (e) to water content. Therefore, the unsaturated behavior of the analyzed clay can be experimentally identified.

- Method for shrinkage measurement in the large clay sample using DIC

The aim is to utilize the DIC technique to measure the shrinkage of a square clay sample (see Fig. 1 and Fig. 2). Note that DIC allows access to both global shrinkage and local strain fields. For measurements, the sample with its support was placed on a scale to measure mass loss during drying and corresponding water content change. The system was housed in a chamber where relative humidity was controlled by salt solutions, maintaining a constant temperature of T = 20°. The descriptive scheme of the experimental device is shown in Fig. 2. Two digital cameras above the device capture sample images every 2 minutes. These images were analyzed using Vic-3D software for displacement and strain field determination.

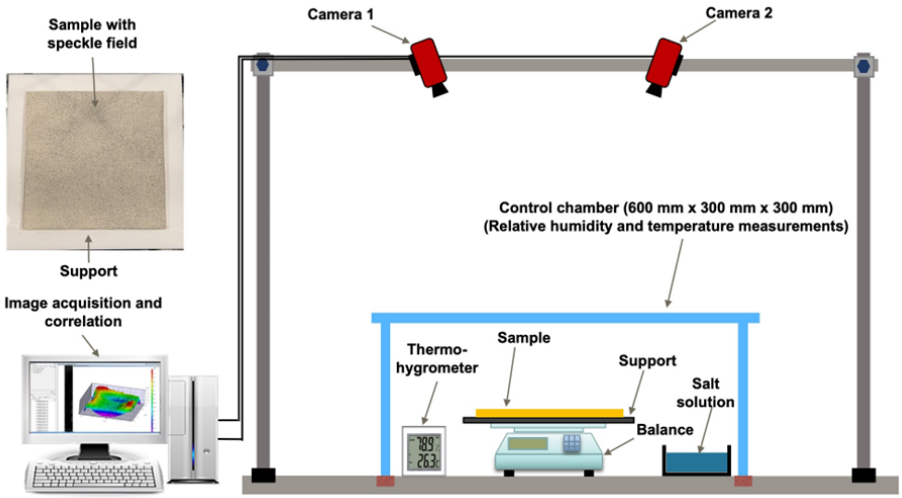

FIGURE 2. Representation of the desiccation test set up

Vic-3D software processes images to generate a contour map. It correlates pixel differences between successive and reference images to derive 3-D displacement and strain fields. Outputs include displacement along X-axis (U), Y-axis (V), and Z-axis (W) in millimeters. An example contour map illustrating the displacement field on the clay sample's surface is presented in Fig. 3.

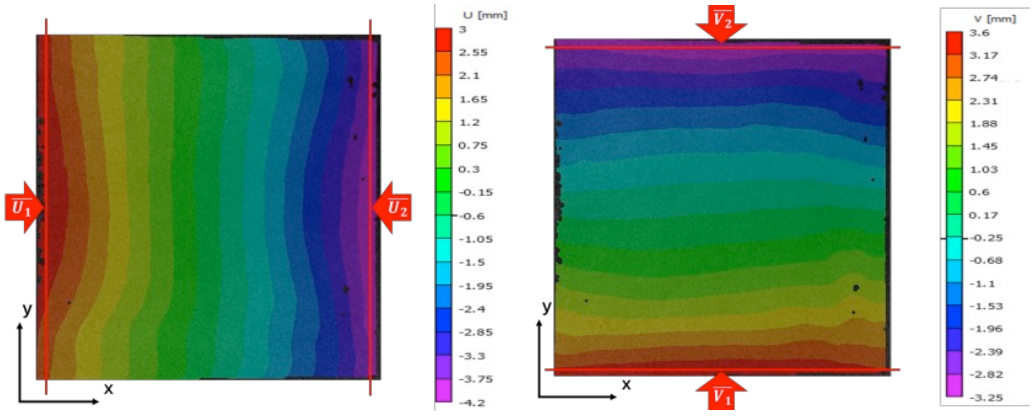

(a) U (mm) Displacement field in x direction (b) V (mm) displacement field in y direction

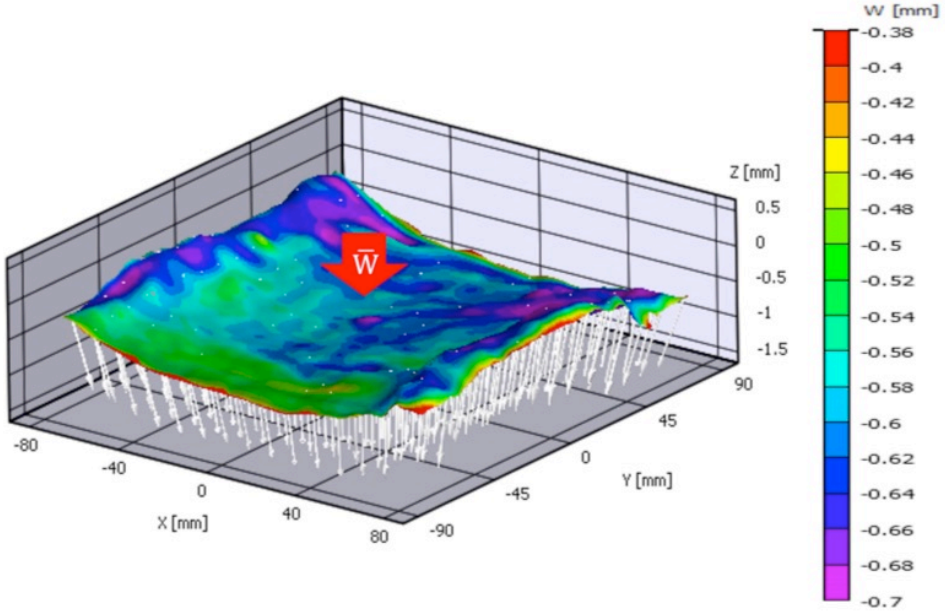

(c) W (mm) displacement field in z direction

FIGURE 3. Example of VIC-3D results in terms of displacement field

results captured at t = 19.6 h of drying with w = 36.1% (Sample size: 179 mm x 179 mm x 5 mm)

Global strains of the sample may be calculated as follows:

$$\varepsilon_x = \frac{\overline{U_1} + \overline{U_2}}{a_0} \qquad \varepsilon_y = \frac{\overline{V_1} + \overline{V_2}}{b_0} \qquad \varepsilon_z = \frac{\overline{W}}{th_0} \qquad Eq.2$$

$\overline{U_1}$ and $\overline{U_2}$ are the average displacement values along the vertical lines on the edge (Fig. 3a), while $\overline{V_1}$ and $\overline{V_2}$ are the average displacement values along the horizontal lines on the edge (Fig. 3b). $\overline{W}$ represents the average displacement value on the analyzed surface (Fig. 3c). a_0, b_0 and th_0 are the initial dimensions of the sample before the shrinkage test.

III. EXPERIMENTAL RESULTS AND CHARACTERIZATION OF THE SHRINKAGE PHENOMENON

A. Soil – Water Characteristic Curve and shrinkage curve

Fig. 4a shows the experimental results of the shrinkage curve of kaolin K13 in the (w-e) plane. Data from Taibi (1994), cited by Wei et al. (2016), were plotted in the same plane. As one can observe, the void ratio evolves as a function of the water content from the initially saturated state till the vicinity of the shrinkage limit (w_{SL}). At this stage, the material is assumed to maintain its saturation, and the curve follows the saturated line defined by $e = G_s \cdot w$. Then, the curve reaches a constant void ratio ($e_{SL} = 0.63$) while w continues to decrease.

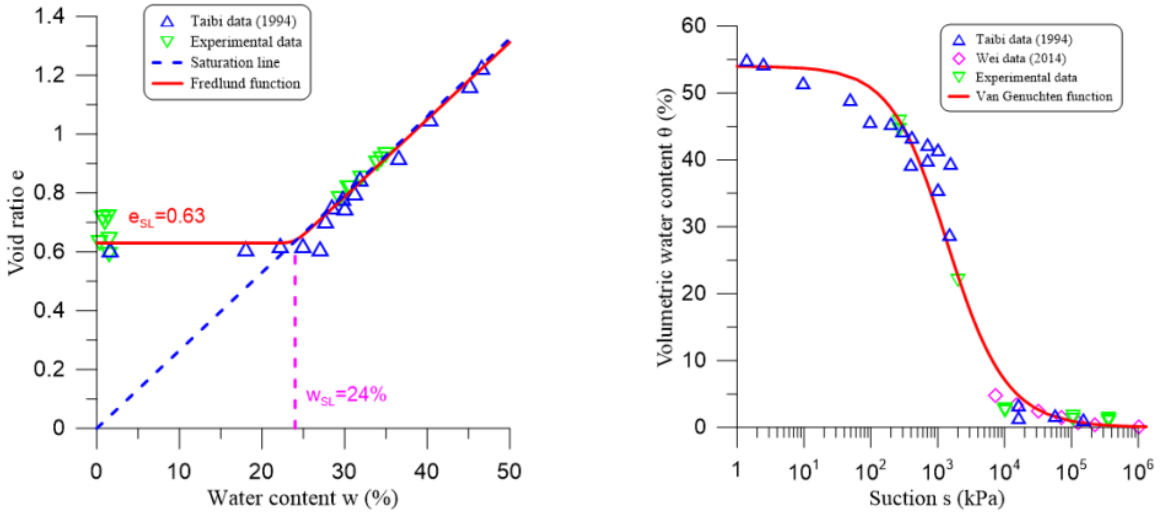

(a) Intrinsic shrinkage line (b) Retention curve

FIGURE 4. Unsaturated properties of the kaolinite

Fig. 4b exhibits the results with those of different authors (Taibi 1994, Wei et al. 2016) in terms of volumetric water content versus suction. Using van Genuchten's law (van Genuchten 1980) expressed by Eq. 6, the experimental data could be fitted.

$$\theta = \theta_r + \frac{\theta_s - \theta_r}{(1 + [\alpha \cdot s]^n)^m} \qquad Eq.3$$

θ is the volumetric water content; s is the suction; θ_r is the residual volumetric water content, 0.001; θ is the saturated volumetric water content, 0.56; n, m and α are parameters related to the soil, where: α = 1000 kPa, n = 1.05 and m = 0.87.

B. Shrinkage identification using DIC global analysis

Drying leads to global strain variations represented in Fig. 5a, using Eq.2 for strain calculations. These results clearly show the development of anisotropic shrinkage, the vertical deformation strain (ε_z) being larger than the strains developed in the two other directions (ε_x and ε_y). It's

noteworthy that, in this scenario, the strain variations in the x and y directions are similar. Upon reaching near-zero water content, strains in all three directions stabilize, with ε_x = 5.8%, ε_y = 5.6%, and ε_z= 16.3%. Towards the end of the drying process, a ratio η of ε_z / ε_x = 2.8 is observed.

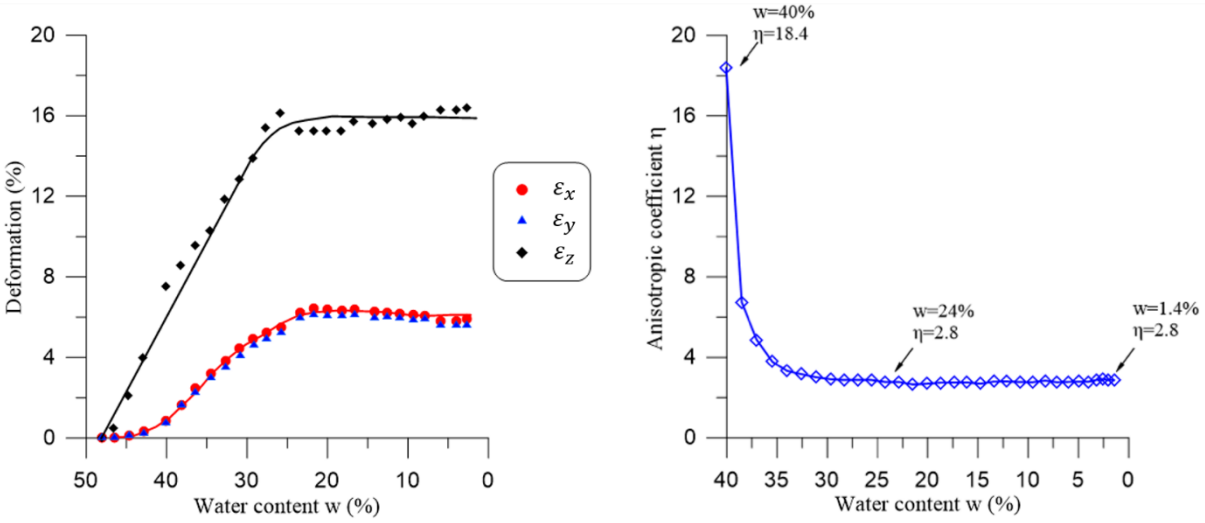

(a) Global strains variation versus water content

(b) Identification of anisotropy parameter as a function of water content

FIGURE 5. Shrinkage of the square surface sample development during drying

Fig. 5b shows the variation of the η parameter that changes from a large value of 18.4, which indicates that the shrinkage starts to develop from the surface of the sample in contact with the imposed RH, to a stabilized value of about 2.8.

C. Shrinkage through local analysis using DIC

During drying, the strain field contour maps on the soil sample surface can be obtained from DIC. From the results, the shrinkage at local scale has been analyzed for different windows P_i, as illustrated in Figs. 6a. Figs. 6b and 6d represent the evolution of the local strains ε_{xx} and ε_{zz}, respectively, versus the water content considering all P_i windows during desiccation.

The results show globally a similar evolution of the local strain curves. At the end of drying, one can observe slight differences between the results of the different windows close to the boundaries and the window in the center. As expected, the trend is that the deformation of the sample surface is larger close to the boundaries and decreases when approaching the center.

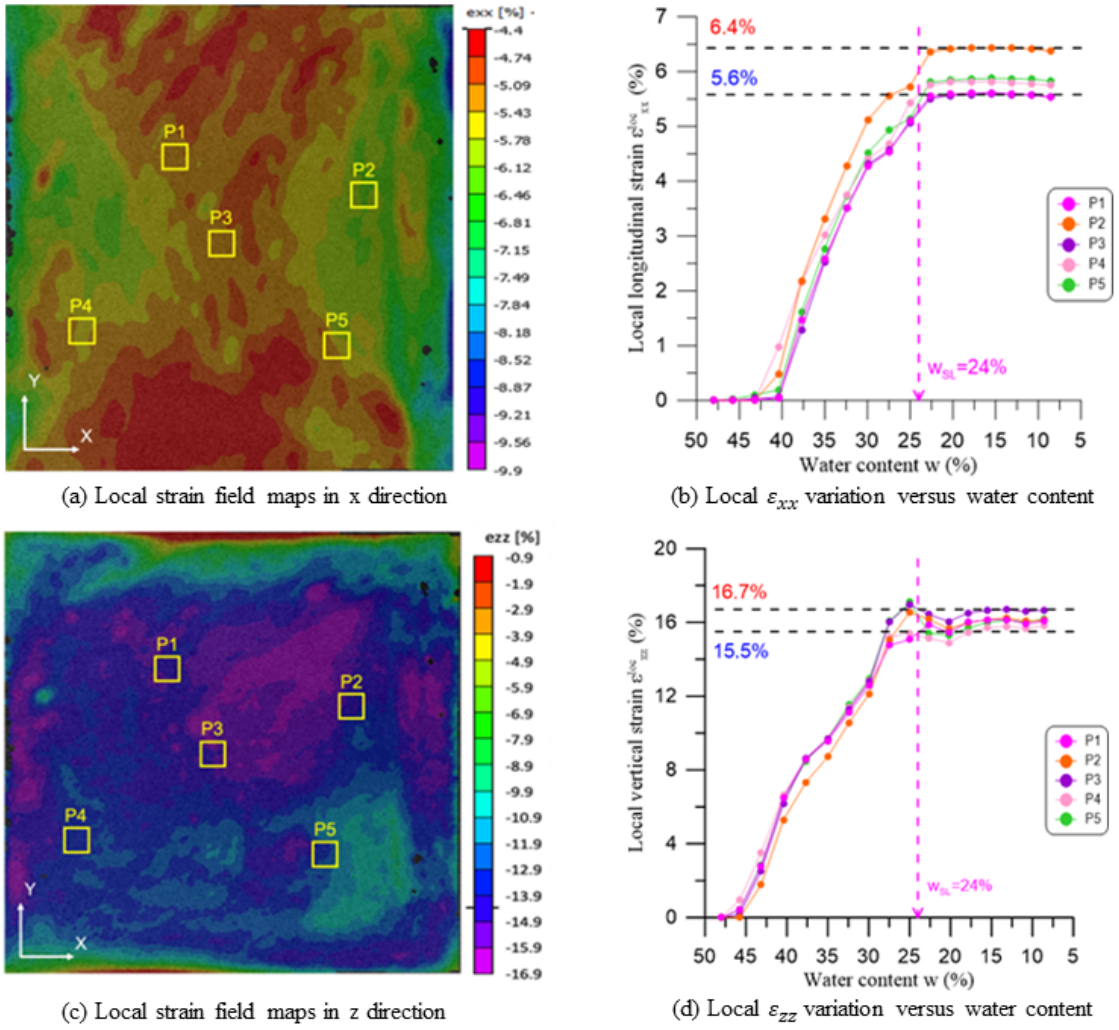

(a) Local strain field maps in x direction

(b) Local ε_{xx} variation versus water content

(c) Local strain field maps in z direction

(d) Local ε_{zz} variation versus water content

FIGURE 6. The experimental results of local vertical strains captured at t = 63h of drying with w= 7.2%

Another effect of drying is associated with the estimated local vertical strain ε_{zz}. In Fig. 6d, larger ε_{zz} values are clearly observed compared to horizontal strain ε_{xx}. In the x-direction, the global deformation of the sample is equal to 5.8%. In the same direction the maximum and minimum values of the local deformation are equal to 6.4% and 5.6% respectively. For the z-direction, the global deformation is equal to 16.3%, while the maximum and minimum values of the local deformation are equal to 16.7% and 15.5% respectively. These results show similar heterogeneity in local deformations in both horizontal and vertical directions. This also highlights an anisotropy similar to that previously obtained at the level global of the sample.

D. Water content distribution in the sample - characterizations from DIC results

From DIC results, one may also determine local volumetric strains by calculating the trace of the local strain tensors:

$$\varepsilon_v^{loc} = \varepsilon_{xx} + \varepsilon_{yy} + \varepsilon_{zz} \qquad Eq.4$$

$$\varepsilon_v = \frac{e_0 - a_0\left[\left(\frac{w}{b_0}\right)^{c_0} + 1\right]^{\frac{1}{c_0}}}{1 + e_0} \qquad Eq.5$$

The local water contents can thus be estimated combining Eq. 4 and Fredlund's equation (Eq. 5), using the adequate Fredlund parameters, where: a_0 = 0.63, b_0 = 0.24 and c_0 = 50. e_0 is the initial void ratio, 1.26.

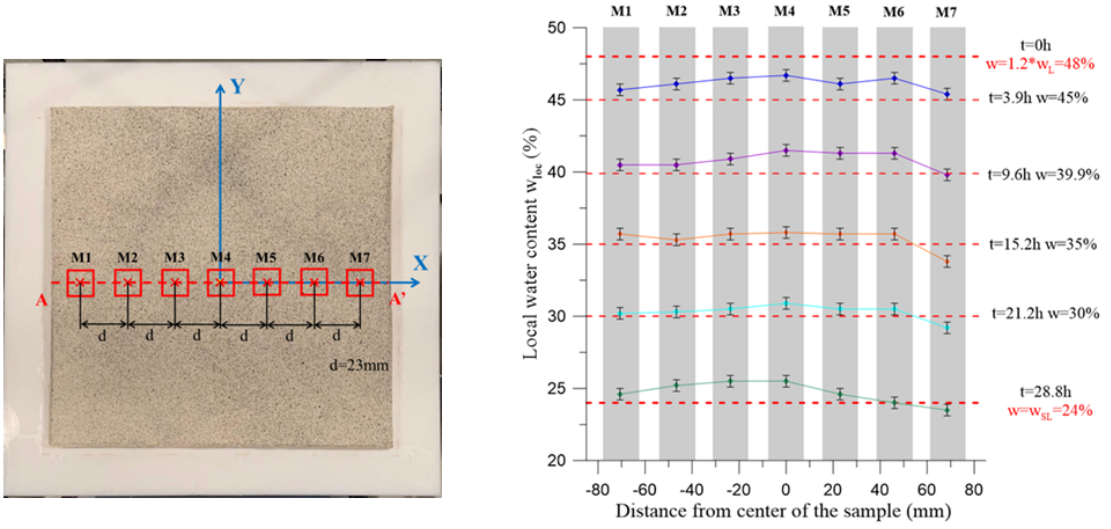

(a) Schematic diagram of selected local water contents (b) Distribution of local water contents

FIGURE 7. Estimation of local water contents from DIC results

Along the AA' line shown in Fig. 7a passing through the sample center, 7 selected zones M_i are first fixed, d = 23 mm being the distance joining the center of two successive zones. Average local water contents can thus be calculated during drying in each zone. The results in Fig. 7b, presenting the water content distribution on AA' line, show that slight local heterogeneities could appear early during drying and, after about 15 h of drying, more visible differences in water content start to appear in the border zone M7. This indicates gradient development in the evolution of water content during drying, from the borders to the center of the sample. In this figure, the discontinuous reds lines correspond to the global water contents obtained through the scale measurements in the global sample.

IV. CONCLUSIONS

The study aimed to analyze the shrinkage phenomenon and estimate the distribution of hydric parameters and their evolution during the drying process of a clay sample using Digital Image Correlation (DIC) technique results. The experimental findings lead to the following conclusions:

1. The soil-water characteristic curve of the tested clay (Kaolin K13) was derived from different experimental tests. Fredlund and van Genuchten curves have been selected as appropriate laws fitting well the shrinkage and retention properties of the material.
2. The developed experimental system effectively observed the shrinkage phenomenon in the square clay specimen. No significant constrained shrinkage that could alter the evolution of free shrinkage or clay/support frictions was observed during the experiment.
3. Anisotropy of shrinkage was experimentally observed in the tested square sample, characterized by the anisotropy parameter η. The vertical component of shrinkage appeared significantly larger than that in the other two directions, while the shrinkage components in the x and y directions were similar.
4. According to the experimental observations permitting to obtain a heterogeneous distribution the water content. This observation suggests the development of gradients in water content evolution during drying, with higher concentrations observed towards the center of the sample.

The study's approach, which relied solely on experimental observations using DIC technique, provided valuable insights into the behavior of clay samples during drying, particularly regarding shrinkage and water content distribution.

REFERENCES

Auvray, R., Rosin-Paumier, S., Abdallah, A., & Masrouri, F. (2013). Quantification of soft soil cracking during suction cycles by image processing. *European Journal of Environmental and Civil Engineering*, 18(1), 11-32.

Cheng, W., Yang, Z., Hattab, M., Bian, H., Bouchemella, S., & Fleureau, J.M. (2022). Free desiccation shrinkage process in clayey soils, *European Journal of Environmental and Civil Engineering*, 26:13, 6398-6423, https://doi.org/10.1080/19648189.2021.1942223

Dyer, M. (2005). Further tests on the fissuring of Thorngumbald flood embankment. *Advanced experimental unsaturated soil mechanics*, ESPERUS 2005, 501–504.

Eid, J., Taibi, S., Fleureau, J.-M., & Hattab, M. (2015). Drying, cracks and shrinkage evolution of a natural silt intended for a new earth building material. Impact of reinforcement. *Construction and Building Materials*, 86, 120–132.

Fleureau, J.-M., Kheirbek-Saoud, S., Soemitro, R., & Taibi, S. (1993). Behavior of clayey soils on drying-wetting paths. *Canadian Geotechnical Journal*, 30, 287–296.

Haines, W. B. (1923). The volume changes associated with variations of water content in soil. *Journal of Agriculture Science*, 13, 293–310.

Lu, N., Godt, J., & Wu, D. (2010). A closed–form equation for effective stress in variably saturated soil. *Water Resources Research*, 46(5), W05515.

Lu, N., Wu, B., & Tan, C. P. (2005). A tensile strength apparatus for cohesionless soils. *Advanced Experimental Unsaturated Soil Mechanics*, 105–110. London: Taylor & Francis Group.

Morris, P. H., Graham, J., & Williams, D. J. (1992). Cracking in drying soils. *Canadian Geotechnical Journal*, 29, 262–277.

Nahlawi, H., Chakrabarti, S., & Kodikara, J. (2004). A direct tensile strength Testing Method for unsaturated geomaterials. *Geotechnical Testing Journal*, 27(4), 356–361.

Péron, H., Delenne, J. Y., Laloui, L., & El Youssoufi, M. S. (2009a). Discrete element modelling of drying shrinkage and cracking of soil. *Computers and Geotechnics*, 36, 61–69.

Péron, H., Hu, L. B., Laloui, L., & Hueckel, T. (2007). Mechanisms of desiccation cracking of soil: Validation. *Numerical Models in Geomechanics–NUMOG X*, 277–282.

Péron, H., Hueckel, T., Laloui, L., & Hu, L. (2009c). Fundamentals of desiccation cracking of fine–grained soils: experimental characterization and mechanisms identification. *Canadian Geotechnical Journal*, 46, 1177–1201.

Péron, H., Laloui, L., Hueckel, T., & Hu, L. B. (2009b). Desiccation cracking of soils. *European Journal of Environmental and Civil Engineering*, 13(7–8), 869–888.

Stirk, G. B. (1954). Some aspects of soil shrinkage and the effect of cracking upon water entry into the soil. *Australian Journal of Agricultural Research*, 5, 279–290.

Taibi, S. (1994). Comportement mécanique des sols soumis à une pression interstitielle négative. *Comptes rendus des Onzièmes Rencontres Universitaires de Génie Civil*, 13–14. Nîmes, France.

Tang, C. S., Cui, Y. J., Tang, A. M., & Shi, B. (2010). Experiment evidence on the temperature dependence of desiccation cracking behavior of clayey soils. *Engineering Geology*, 141 (3–4), 261–266.

Tang, C. S., Shi, B., Liu, C., Suo, W. B., & Gao, L. (2011). Experimental characterization of shrinkage and desiccation cracking in thin clay layer. *Applied Clay Science*, 52, 69–77.

Tempany, H. A. (1917). The shrinkage of soils. *Journal of Agricultural Science*, 8, 312–330.

Van Genuchten, M. T. (1980). A closed–form equation for predicting the hydraulic conductivity of unsaturated soils. *Soil Science Society of America Journal*, 44, 892–898.

Wang, D.Y., Tang, C.S., Cui, Y.C., Shi, B., & Li, J. (2016). Effects of wetting drying cycles on soil strength profile of a silty clay in micro–penetrometer tests. *Engineering Geology*, 206, 60–70.

Wei, X., Hattab, M., Bompard, P., & Fleureau, J.-M. (2016). Highlighting some mechanisms of crack formation and propagation in clays on drying path. *Géotechnique*, 66(4), 287–300.